prosthesis

MDPI

Article

Customized Wrist Immobilization Splints Produced via Additive Manufacturing—A Comprehensive Evaluation of the Viable Configurations

Francesca Sala *, Gianluca D'Urso and Claudio Giardini

Department of Management, Information and Production Engineering, University of Bergamo, 24044 Dalmine, Italy; gianluca.d-urso@unibg.it (G.D.); claudio.giardini@unibg.it (C.G.)
* Correspondence: francesca.sala@unibg.it

Abstract: Orthopedic splints are external medical devices designed to support and protect the functions of the human musculoskeletal system from pathological conditions or traumatic events. Tailoring these medical solutions to the morphology of the patient's limb is essential to ensure a correct and rapid rehabilitation pathway. Although traditional splinting techniques might achieve a unique fit, the procedures are highly dependent on the skill and experience of the medical operator, affecting the quality of the care treatment. In response to the drawbacks associated with traditional splinting techniques, the present article proposed an innovative and structured methodology to manufacture customized wrist immobilization splints, prioritizing simplicity and user-friendliness in fabrication activities. The customized splint manufacturing was based on the integration of reverse engineering (RE) and additive manufacturing (AM) techniques. The research designed a baseline model of a wrist splint, varying over different thickness values and manufacturing materials (ABS, nylon, PLA, PC, PA6-GF25, PA6-CF20). For every splint model, the production times and material costs were assessed. Technical tests were performed via finite element analysis (FEA). The conducted analysis and the resulting charts empower medical operators to select the most appropriate solution, ensuring a well-informed and effective decision-making approach.

Keywords: reverse engineering; additive manufacturing; fused deposition modeling; orthosis; wrist splint; finite element analysis

Citation: Sala, F.; D'Urso, G.; Giardini, C. Customized Wrist Immobilization Splints Produced via Additive Manufacturing—A Comprehensive Evaluation of the Viable Configurations. *Prosthesis* **2023**, *5*, 792–808. https://doi.org/10.3390/prosthesis5030056

Academic Editor: Marco Cicciu

Received: 21 June 2023
Revised: 23 August 2023
Accepted: 24 August 2023
Published: 26 August 2023

1. Introduction

Splints, often referred to as orthoses or braces, are defined as external orthopedic devices intended to restore the physiological functions of the human musculoskeletal apparatus [1]. Upper extremity splints are distinguished on the basis of descriptive criteria, such as the primary purpose [2,3]. In compliance with the therapeutic target and clinical protocol established for a given pathological condition, splints are classified into mobilization, immobilization, restriction, and torque transmission splints.

The wrist is one of the upper extremity structures most frequently treated with splinting solutions. The use of wrist splinting is often advocated in clinical conditions involving carpal tunnel syndrome, radial nerve injuries, tendinitis and tenosynovitis, rheumatoid arthritis, wrist fractures and sprains, complex regional pain syndrome type I, and joint contractures. In treating these pathologies, therapists rely on a range of wrist immobilization splints that are able to maintain wrist structures in the correct alignment while simultaneously allowing a certain grade of finger mobility [4].

Physicians have at their immediate disposal prefabricated wrist splints designed to fit on a large population scale. Nevertheless, these solutions rarely adhere to the individual patient's morphology optimally, requiring modifications that are not always feasible. In addition, adjustments may compromise the functionality of the device and consequently hin-

der the patient's rehabilitation pathway. As a matter of fact, the partial or total lack of control over the wrist angle positioning in a prefabricated splint results in adverse outcomes [5–7].

In response to the major disadvantages associated with off-the-shelf splints, therapists fabricate customized wrist immobilization splints using low-temperature thermoplastic (LTT) materials. The production process is heterogeneous and demanding: it is performed by a trained medical professional, and sometimes it may require the assistance of a second operator to ensure the correct positioning of the patient's limb. Generally, the arm of the patient is placed in a neutral resting position on a sheet of paper on which the pattern (e.g., volar, dorsal, ulnar, or circumferential) of the wrist immobilization splint is traced. Once the adequacy of the pattern is checked, it is transferred onto a film of LTT material, which is softened in hot water (60 °C to 80 °C temperature), trimmed, and molded directly onto the skin of the patient. Additional adjustments are always required, and closures are implemented at the end of the splinting process. As a result, the customization, prompted by the individual diagnostic case, is enhanced by the splinting practice diversification derived from the physician's expertise.

Although the fabrication of custom splints provides a unique and specific therapeutic treatment for the patient compared to universal splints, the approach is not free of flaws. The customized splinting process is severely dependent on the skills, experience, and preferences of the healthcare operator [8], jeopardizing the quality of the medical device. In fact, it has been demonstrated [9] that thermal injuries and pressure-related complications (e.g., decreased blood perfusion and compartment syndrome) are more frequent when the splinting process is performed by less experienced practitioners. Therefore, taking into consideration the preceding argumentations, the present study outlined an innovative methodology to fabricate patient-specific wrist immobilization splints. The proposed fabrication methodology addressed the variability induced by disparate levels of medical expertise by structuring and standardizing the custom splinting process through the integration of advanced techniques and technologies in traditional medical practice. The benefits from prefabricated and custom splints were brought together so as to obtain devices characterized by a steady, high standard of quality and a great degree of customization. The emphasis was posed on the relevance of delivering optimal care by enhancing the individuality of the patient's requirements with non-traditional methodologies: The lightness, strength, comfort, availability, and affordability of the splint solutions were concomitantly valued and balanced in an effort to provide satisfactory outcomes.

In the present research, a tailor-made splint was fabricated from the morphology of the patient's arm: the geometry of the wrist was acquired through reverse engineering techniques. Advancement in this field promoted the diffusion and utilization of 3D scanner solutions in human modeling and especially in upper limb modeling. Scientific studies [10] demonstrated that optimal reconstructions were performed using handheld scanners, characterized by fast acquisition time. Additionally, the early apparatus [11–13], encompassing multiple cameras arranged in a circular frame, was developed and reconstructed the patient's limb via an instant acquisition. A similar approach [14] involved a single camera attached to an arm that rotates in a circular motion around the patient's limb. In opposition, traditional medical techniques, like computed tomography (CT) and magnetic resonance imaging (MRI), were considered inappropriate with respect to the current objective. Besides their great investment cost and limited availability in health care facilities, these techniques were invasive and not always executable on the patient.

Once scanned, the patient's limb was translated into the digital copy of a customized wrist immobilization splint. Given the significant importance and intricate nature associated with the conversion process of scanned data into a simple and straightforward 3D printable model, it becomes imperative to emphasize, as an alternative to purely manual modeling, the availability of diverse methods for conducting this process [15–17]. The current study based the modeling activity on a dedicated software based on the Python language [18]. The application was developed with the aim of replacing the manual modeling activities [19–21] commonly performed by CAD technicians when elaborating the

scanned information of similar medical applications. Thus, modeling time and effort were minimized, and technical knowledge of CAD software was no longer required. Conceived with a user-friendly interface, the considered software comprises a set of intuitive commands that grant physicians a fair degree of arbitrariness in splint designing without affecting the quality of the final model.

The realization of the physical prototype of the wrist immobilization splint was carried out by means of additive manufacturing (AM) techniques, highly automated manufacturing processes able to realize complex geometries with reduced human intervention [22]. These technologies were seen as viable options to meet the customization needs sought in the traditional splinting procedure. In particular, the manufacturing of the device was based on a desktop fused deposition modeling (FDM) 3D printer and a range of biocompatible filaments, both polymeric and composite materials. This technology is based on the principle of material extrusion: a thermoplastic filament is heated through a head nozzle and deposited layer upon layer according to a precise pattern and a meticulous selection of the process parameters [23–25] onto a build platform where the material cools and solidifies and gradually builds the final 3D structure. In the literature, FDM was used in the prototyping of a variety of skin-contact orthopedic devices, ranging from neck braces [26,27] to ankle–foot orthoses and insoles [28–31]. Upper limb splints and casts were primarily based on fused filament fabrication (FFF) printers [32–34].

Along with the definition and integration of the activities for an easy, effective, and clinician-friendly manufacturing approach of patient-specific splints for wrist immobilization, the present work comprised the execution of analyses evaluating the feasibility of the intended process and product. The present research aimed at assessing, in a comprehensive way, the applicability of the proposed methodology and the derived products in clinical practice. Particularly, the sustainability of the process was measured in terms of time and cost by focusing attention on the minimization of production times and material costs. Moreover, the compliance of the prototypes resulting from the discussed manufacturing process was assessed via finite element analysis (FEA): stresses and displacement distribution maps were presented. The FEA results were discussed in relation to the performance characteristics typically sought by clinicians during the splinting process.

Lastly, the present research quantified and displayed the outcomes of the feasibility analysis as a comparative collection of wrist immobilization splint configurations at the disposal of the physician for the treatment of the pathological wrist condition. The heterogeneity of the factors considered in the benchmark resulted in a comprehensive evaluation of the wrist immobilization splint configurations, and to date, such an assessment was not yet discussed in the literature.

From a broader perspective, this research showcased the vital role that scientific methodology and adopted technological innovation play in shaping the future of health care: the integration of medical knowledge and manufacturing engineering contribute to the advancement of medical science and patient care.

2. Methodology

2.1. Reconstruction of Wrist Geometry

The scanning procedure was performed using Hexagon Absolute Arm 7-Axis equipped with RS6 Laser Scanner. The contactless acquisition system consists of a handheld scanner (technical characteristics are shown in Table 1) set on a portable measuring arm.

The orientation and positioning of the patient's wrist for personalized splint development varies depending on the diagnosis and therapeutic goals. In the present study, the wrist configuration adopted was a neutral resting position, typically used in the treatment of carpal tunnel syndrome. In practice, the patient was asked to sit still with the arm raised frontally so that the points that identify the shoulder and wrist joints were aligned on the same axis. The stability of the configuration was fostered by placing two supports of equal height in the proximity of the elbow joint and under the fingertips. The conceived configuration optimally exposed the external geometry of the patient's upper limb, pre-

venting shape distortion associated with arrangements that instead involve resting the arm on a surface. Additionally, the contactless systems avoided exposing the patient's limb to additional stresses and helped the patient hold the correct position comfortably.

The position of the patient during the reconstruction of the wrist morphology is represented in Figure 1.

The scansion was executed as a single 360-degree acquisition around the patient's upper limb, avoiding unnecessary complications in merging multiple scans.

Few attempts were performed before selecting the finest result. Files with slight misalignments and/or discontinuities in the point cloud were further processed and correctly elaborated. Compromised files were discarded. The average scanning time to acquire the current anatomical district was around 110 s, but it is worth mentioning that this value may vary since it relies on the skills of the operator.

Figure 1. Position of the patient during the reconstruction of the wrist geometry. The blue rectangles identify the position of the supports providing stability.

Table 1. RS6 Laser Scanner characteristics—Hexagon technical data sheet [35].

RS6 Laser Scanner	
Scanning technology	blue laser
Scanning accuracy	0.026 mm
Point acquisition rate	max. 1.2 million points/s
Points per line	max. 4000
Line rate	max. 300 Hz
Line width	150 mm

2.2. Design of the Wrist Immobilization Splint Model

Starting from the 3D acquisition of the patient's wrist, an STL model of a circumferential splint was designed using CAD software based on Python libraries. The authors introduced the software system, which was conceived to address the specific needs and challenges of the field in a previous article [18]. The application optimizes and streamlines the process of manual modeling into a set of intuitive and user-friendly commands (Figure 2) that were specifically developed for clinical practitioners' use.

The first operation automates the translation of the model to the origin of the workspace reference system, the repair of the mesh geometry errors (such as holes, gaps, intersections, and floating triangles), and the surface smoothing. These activities improved the quality of the mesh by addressing potential artifacts resulting from the 3D scanning activity and by preparing the file for the subsequent modeling operations. Once the mesh geometry

was corrected, two offsets were applied: the first one expanded the model surface outward and was designed to ensure clearance between the arm and the inner surface of the device, while the second one generated the solid shape by imposing a surface thickness. The user is required to input the offset value to ensure that the resulting orthotic device is tailored specifically to the needs of the patient. The cut and rotate commands refine the splint model, removing the non-functional areas. To accurately orient and section the model, the operator relies on the numerical values displayed by a protractor and millimeter grid. Ventilation holes were created to lighten the structure while providing sufficient strength. From a library that includes ventilation holes with distinct shapes, the user chooses the hole and applies it to the model either by selecting the location or by creating a pattern of evenly spaced holes. In the final stages of the modeling activity, the splint model was divided into two complementary shells and integrated with fastening systems. Given the circumferential design of the medical device, these operations are necessary in order to ensure that the patient is able to fit the splint and lock it in place. The algorithms and consequently the interfaces of the division and closure commands recall the removal of unnecessary parts and creation of ventilation holes, respectively. The outputs of the modeling activity were two STL files representing the two halves of the medical device.

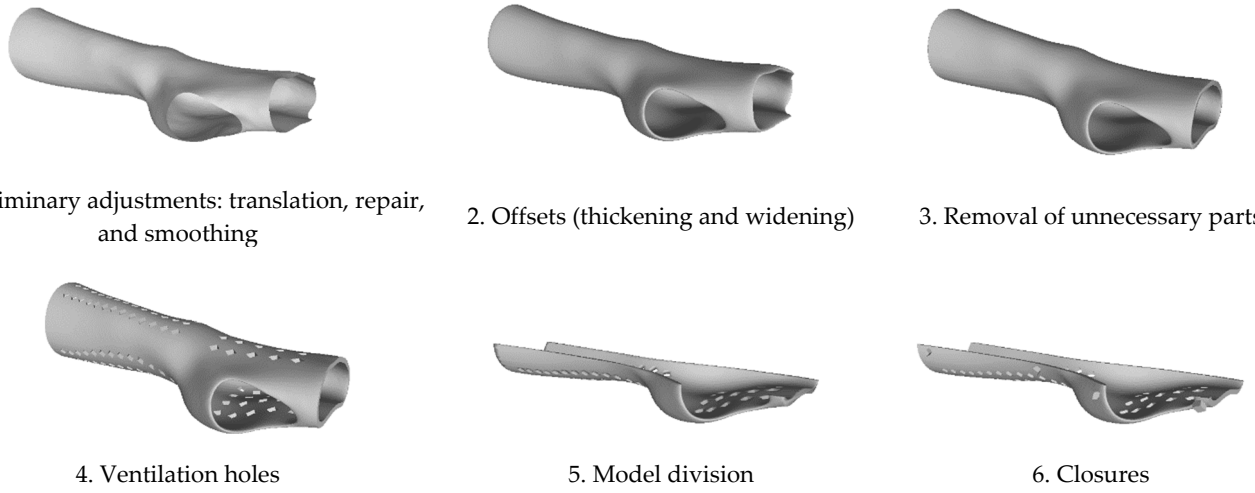

Figure 2. Flowchart of the guided modeling operations.

2.3. Production of the Splint Prototype

The splint prototype was conceived to be realized with an instrument able to easily fabricate customized and intricate geometries. Fused deposition modeling (FDM) represents the appropriate process for the intended purpose, as well as being easily implementable in any health care setting. The considered printer was an Ultimaker S5 desktop-FDM (Ultimaker B.V., Utrecht, NL, USA) with a working chamber of 330 × 240 × 300 mm. The technology is equipped with a double extruder: one extruding the primary material and the other extruding the support material. Different sets of print cores were used depending on the print material.

The manufacturing materials were chosen in compliance with the biocompatibility requirements. Splints represent medical devices that interface with the patient's body superficially, and the contact occurs on intact skin for an extended duration. The indications to which this type of medical device is subjected during the biological evaluation include assessing issues related to cytotoxicity, sensitization, and intra-cutaneous irritation or reactivity [36]. For this type of medical application, some materials identified by the FDA as low-risk materials do not require any testing for pre-market submission [37] and, consequently, were considered in the study. Additional materials not belonging to the above category were taken into account. Composites, such as glass-reinforced and carbon-

reinforced polymers, were included in this study given their enhanced properties: high stiffness and strength while maintaining lightness.

ABS, nylon, PLA, and PC filaments were provided by Ultimaker [38–41], while PA6-GF25 and PA6-CF20 filaments were provided by Polymaker [42,43]. The chosen support material was Ultimaker Breakaway [44], a filament composed of a mixture of PLA and TPU. Besides being compatible with the majority of the selected material, Ultimaker Breakaway is quickly and manually removable at the end of the printing process.

Polymeric filaments, including the support filament, necessitated the utilization of a regular print core (AA-type) that comes with a nozzle size of up to 0.8 mm. Conversely, composite filaments mandate the use of hardened steel print cores (CC-type) designed for handling abrasive or composite materials. These print cores are available with a maximum nozzle size of 0.6 mm.

2.4. Time and Cost Analysis

The overall process time for producing a customized splint device via additive manufacturing included the execution of the activities of limb scanning, splint CAD-model development, and splint printing. The 3D printing task, also considered the most time-consuming activity, was estimated from the STL model of the medical device through a 3D slicing application for 3D printers (Ultimaker Cura). The calculation of the time for printing a splint prototype was performed using specific printing parameters for each selected material filament (Table 2) in accordance with the recommended printing settings [42–48].

Table 2. FDM filaments printing parameters.

	ABS	**Nylon**	**PLA**	**PC**	**PA6-GF25**	**PA6-CF20**
Nozzle diameter	0.8 mm	0.8 mm	0.8 mm	0.8 mm	0.6 mm	0.6 mm
Layer height	0.6 mm	0.6 mm	0.6 mm	0.6 mm	0.45 mm	0.45 mm
Infill density	100%	100%	100%	100%	100%	100%
Infill pattern	Line	Line	Line	Line	Line	Line
Nozzle temperature	250 °C	245 °C	210 °C	265 °C	300 °C	300 °C
Build plate temperature	85 °C	70 °C	60 °C	110 °C	50 °C	50 °C
Print speed	50 mm/s	35 mm/s	45 mm/s	70 mm/s	60 mm/s	60 mm/s

The diameter size of the head nozzle extruding the primary material was chosen to maximize the height of the deposited layers: a 0.8 mm head nozzle was selected for polymeric filaments, while a 0.6 mm was selected for the composite materials. The chosen layer heights, 0.6 mm and 0.45 mm, respectively, implied a considerable reduction in printing time and a rougher surface compatible with the intended solution. The infill density was set at a constant level of 100%, whilst the infill pattern type was set as lines. The chosen printing speed was the default one.

The minimum angle of overhangs for which support material was added was 80°, which reduced the utilization of the support material to a minimum by depositing it just in correspondence of the opening dedicated to the thumb finger. Furthermore, the support material infill density was reduced to 10%, and the pattern type was set as triangles.

The two complementary shells of the splint model were positioned on the printing plane vertically to further reduce the printing time along with the reduction in the consumption of the support material.

Based on existing models specifically developed for estimating the costs involved in the fabrication process of customized orthotics [18], leading cost items were identified. The total cost of a tailor-made orthosis is driven by labor costs and material costs. Machining costs, including technologies purchase cost (3D scanner and 3D printer) and energetic cost, represent a fraction of the overall cost.

Besides labor cost, the most impactful cost item is material cost, obtainable from the information on material cost and material consumed during the 3D printing process. The 3D slicing software for 3D printers, Ultimaker Cura, gave the length value of material

extruded during printing. The estimate came from the printing arrangements presented in Table 2, which, in addition to shortening printing times, optimized the amount of extruded filaments, reducing the cost of raw material. In the present research, the computation of material cost components excluded corrections due to factors such as material waste and scrap and fluctuation in raw material prices.

Both time and cost analyses followed the programming of the experiments, design of experiment (DOE), in which two factors, splint thickness and manufacturing material, were varied on 3 and 6 levels, respectively.

2.5. Technical Analysis

The commercial availability of different thermoplastic materials allows the physician to further tailor the splint, keeping in mind that the selection of the most suitable material involves comparing the therapeutic targets with the technical characteristics of the manufacturing material. Conformability, flexibility, durability, rigidity, and design appearance (e.g., ventilation, color, thickness, and finish) [4] are the technical characteristics sought by medical personnel.

Mechanical properties of the medical devices produced with the designed AM procedure were evaluated through the execution of finite element analysis (FEA) using Abaqus. Splint STL models differing in surface thickness were developed during the CAD modeling phase and loaded into Abaqus working space.

The models were subjected to a free technique meshing process: the algorithm automatically adapts the size and shape of the elements to accurately represent the local features, ensuring great flexibility in capturing the complexity of the current geometry. Models were discretized using tetrahedral elements characterized by an approximate global size ranging from 2.5 mm to 5.5 mm depending on the necessity to cope with possible convergence and numerical instability problems during the execution of the simulation. The resulting mesh consisted of a total of 86,743 elements for splint model of 2 mm, 127,455 for splint model of 3 mm, and 140,326 elements for splint model of 4 mm. The number of nodes was 164,583 for splint model of 2 mm, 217,929 for splint model of 3 mm, and 234,339 for splint model of 4 mm.

The mechanical properties of the splint model were tested according to different manufacturing materials. The selected materials were the standard and fiber-reinforced polymeric materials presented in Section 2.3, and the simulations were set up with the material properties [38–43] reported in Table 3.

Table 3. Mechanical properties of the manufacturing materials.

	ABS	**Nylon**	**PLA**	**PC**	**PA6-GF25**	**PA6-CF20**
Mass density	1.10 g/cm^3	1.14 g/cm^3	1.24 g/cm^3	1.20 g/cm^3	1.20 g/cm^3	1.17 g/cm^3
Young's modulus (E)	1 682 MPa	579 MPa	2 347 MPa	1 904 MPa	4 431 MPa	7 453 MPa
Poisson ratio (ν)	0.35	0.39	0.33	0.36	0.40	0.38
Ultimate tensile strength (UTS) after 3D printing	33.9 MPa	34.3 MPa	45.6 MPa	53.7 MPa	84.0 MPa	105.0 MPa

As noted in other bibliographical research [13,20,21], explicit strength requirements are lacking. Additionally, upper limb splints are not subjected to specific and/or elevated mechanical loads; therefore, this study simulated an unintentional mechanical impact. The simulation specifically focused on recreating the collision of the palm region of the medical device against a surface during a patient fall episode while wearing the designed device. Load and constraint conditions were carefully established in order to ensure an accurate representation of the aforementioned scenario. The test was performed by constraining the displacements and rotations of the nodes describing the region close to the distal part of the ulna and imposing a pressure uniformly distributed over the palm surface (with a total magnitude of 500 N). The minimum thickness demonstrating sufficient strength

was identified for each material. Additionally, displacements affecting the wrist area were reported. The recorded results were attributable to the system consisting of the mere splint, meaning that the tests were performed without simulating the presence of the arm inside the medical device.

3. Results and Discussion

3.1. Results

Following the methodology presented in Section 2.2, from a single 3D acquisition, three splint models were designed. All the splint models include a pattern of rhomboidal holes designed to facilitate the ventilation function and lighten the entire structure. The modeling parameters during the CAD stage were kept unchanged except for the offset parameter, which is responsible for creating the solid shape of the scanned surface. Therefore, the three splint models present the same general conformation, while the surface thickness was varied by 2, 3, and 4 mm, respectively. The time, cost, and technical analyses were based on the use of 6 different manufacturing materials, thus, resulting in a total of 18 splint combinations.

As presented in Section 2.4, the splint models were evaluated in terms of time and costs, leveraging the Ultimaker Cura slicing software version 5.3.0. The printing time (Figure 3) and the amount of extruded material (Tables 4 and 5) of the 18 splint combinations were simulated. From the information on the extruded material, the material weight and material cost (Figure 4) were derived. The material weight considered only the manufacturing material, whilst the material cost also included the cost component of the support material.

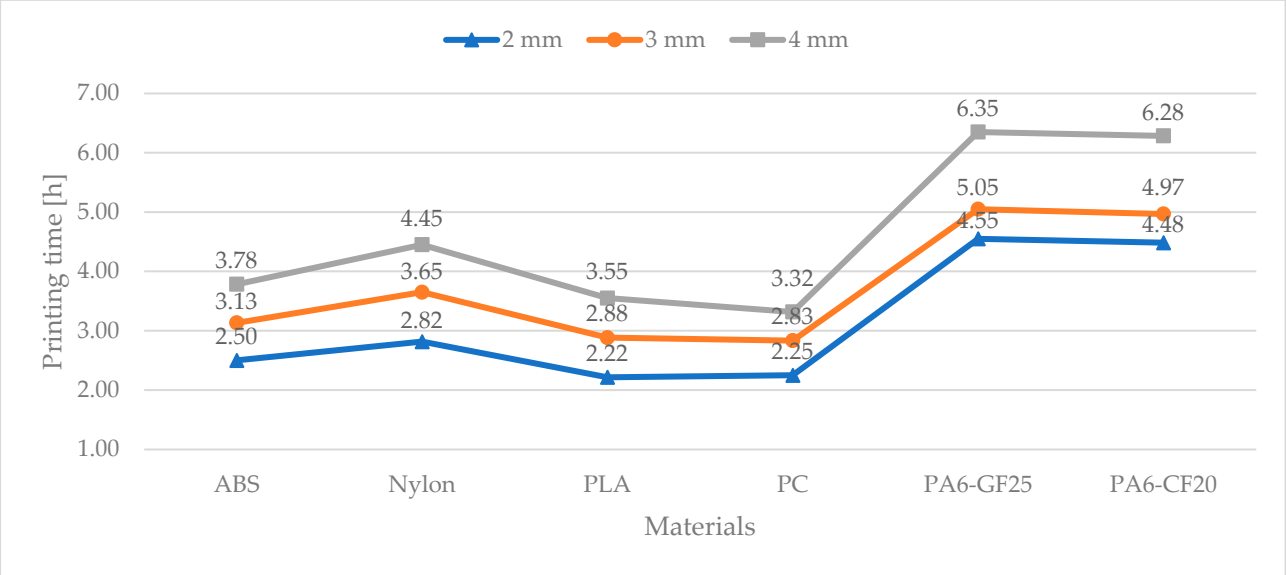

Figure 3. Printing times for producing a customized wrist immobilization splint as a function of the material type and thickness. ABS, nylon, PLA, and PC filaments used a head nozzle of 0.8 mm in diameter, while PA6-GF25 and PA6-CF20 used a head nozzle of 0.6 mm in diameter.

Table 4. Manufacturing material consumptions and manufacturing material prices (support material not included).

	ABS	Nylon	PLA	PC	PA6-GF25	PA6-CF20
Material consumption, 2 mm	10.95 m	10.91 m	10.97 m	11.08 m	10.98 m	10.83 m
Material consumption, 3 mm	16.51 m	16.48 m	16.55 m	16.65 m	16.81 m	16.67 m
Material consumption, 4 mm	22.61 m	22.58 m	22.66 m	22.75 m	22.95 m	22.81 m
Material price	0.58 €/m	0.92 €/m	0.57 €/m	0.90 €/m	1.38 €/m	1.64 €/m

Table 5. Support material consumption and support material price. Ultimaker Breakaway was used as support material.

	For ABS	For Nylon	For PLA	For PC	For PA6-GF25	For PA6-CF20
Support consumption, 2 mm	0.21 m	0.28 m	0.23 m	0.20 m	2.39 m	2.39 m
Support consumption, 3 mm	0.20 m	0.21 m	0.19 m	0.20 m	0.90 m	0.90 m
Support consumption, 4 mm	0.20 m	0.20 m	0.22 m	0.16 m	0.97 m	0.96 m
Support price	0.92 €/m	0.92 €/m	0.92 €/m	0.92 €/m	0.92 €/m	0.92 €/m

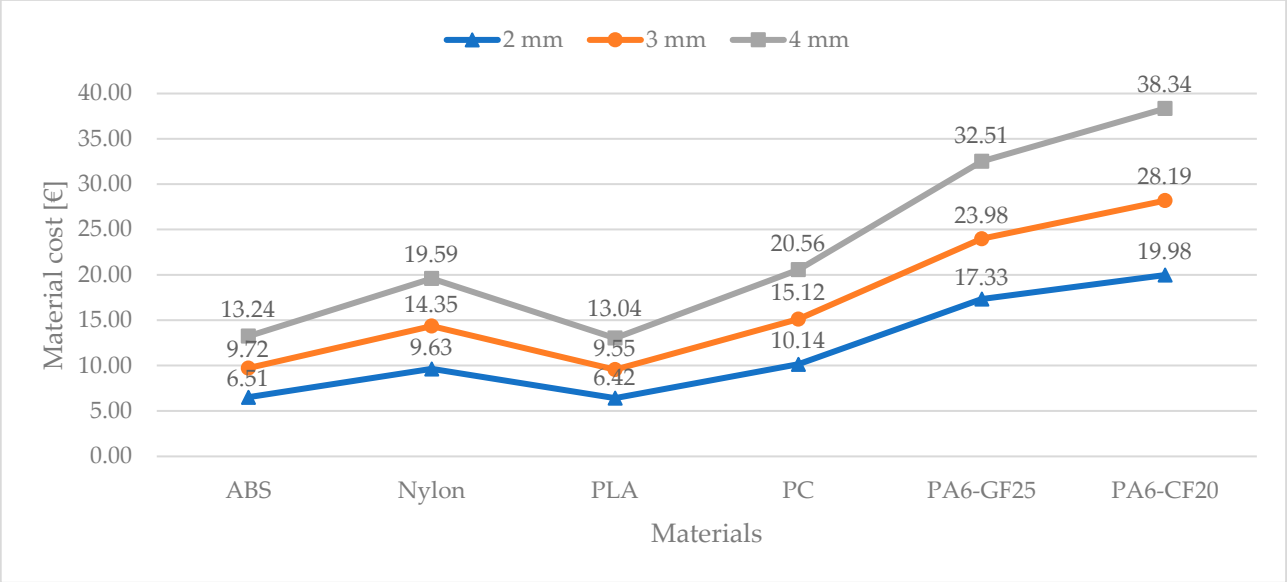

Figure 4. Total material cost for producing a customized wrist immobilization splint as a function of the material type and thickness (the values include both the manufacturing material component and the support material component).

Technical analysis was performed: FEA provided the predicted stresses and displacement distribution maps of the wrist immobilization splint, which were consistent across all scenarios given their sole dependence on geometric factors. For each experiment, the expected maximum stress value was recorded in correspondence of the opening area dedicated to the thumb finger, as shown in Figure 5. The maximum values of stress were averaged to 64 MPa for a splint configuration of 2 mm, 28 MPa for a splint configuration of 3 mm, and 18 MPa for a splint configuration of 4 mm. The results are presented in Figure 6 where they are compared to the UTS of each manufacturing material in order to identify the splint combinations capable of withstanding the simulated accidental mechanical impact: the maximum stress values exceeding the material UTS result in splint failure. It is critical to mention that all 18 splint combinations, near the apexes of the ventilation holes, showed a stress intensification effect, which might be limited through the implementation of a fillet radius on every angle of the rhomboidal shape hole.

Concerning displacements, the distribution maps of the 18 splint combinations followed a pattern like the one depicted in Figure 7. Table 6 reports the range of the displacement values impacting only the wrist area.

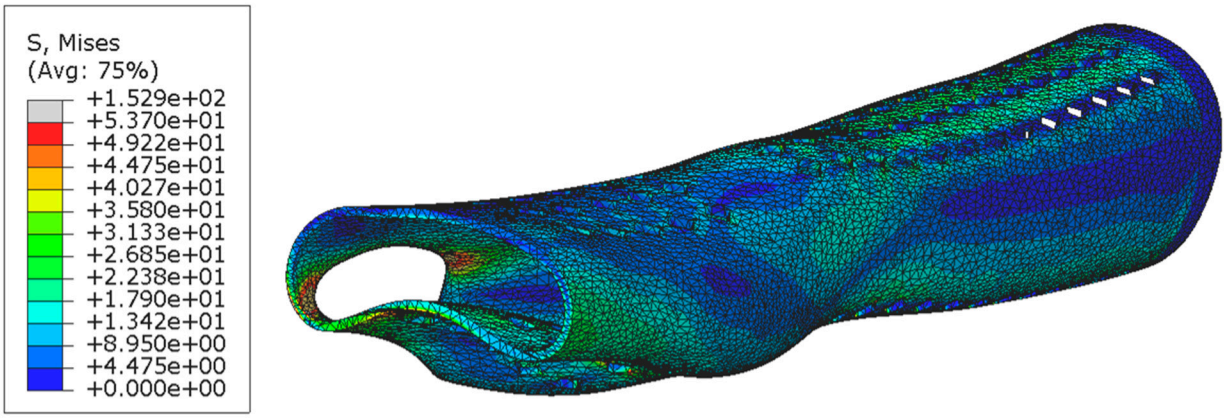

Figure 5. Von Mises stress distribution for PC wrist immobilization splint with a 2 mm thickness.

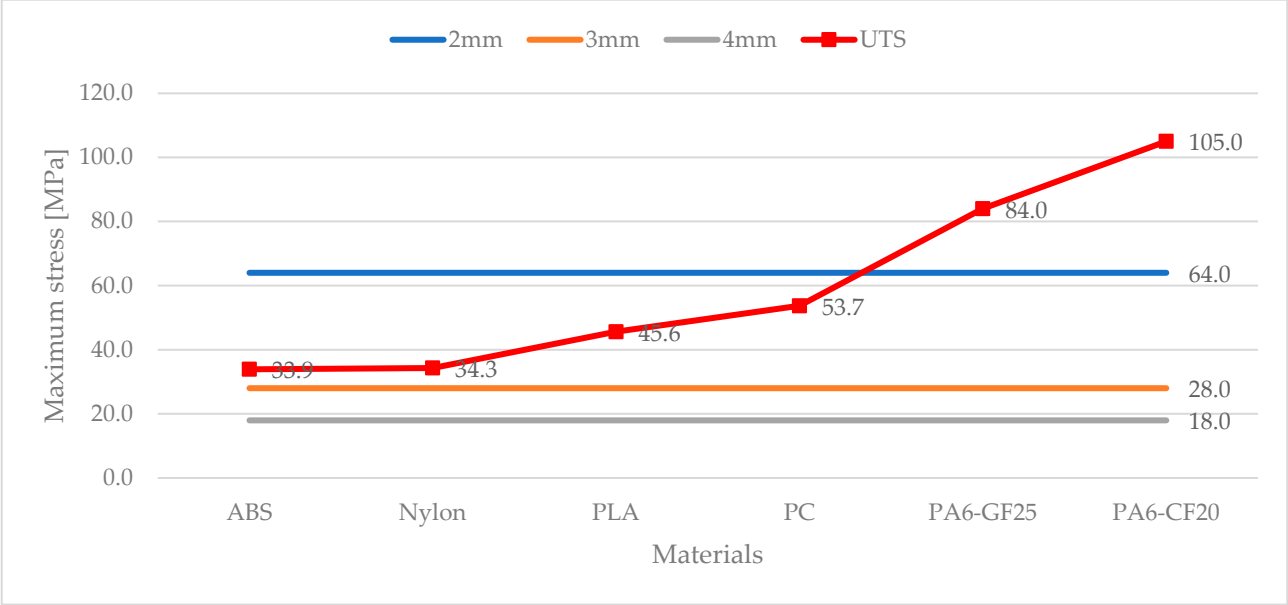

Figure 6. Maximum value of stress experienced by the splint model according to splint thickness (2, 3, 4 mm) compared to the UTS of each material type (ABS, nylon, PLA, PC, PA6-GF25, PA6-CF20).

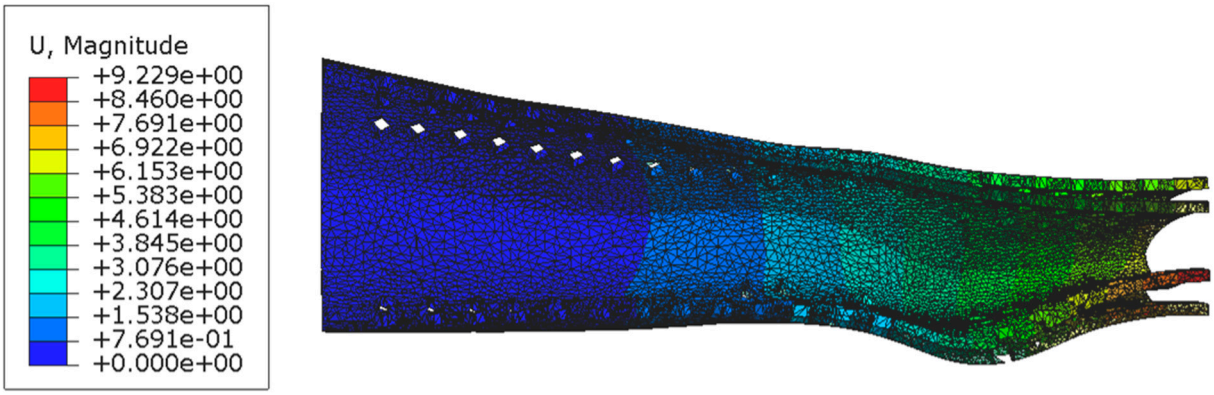

Figure 7. Displacement distribution for PC wrist immobilization splint with a 3 mm thickness.

Table 6. Range of displacement according to material filament and splint thickness.

	2 mm	3 mm	4 mm
ABS	3.9–7.8 mm	2.6–4.4 mm	1.8–2.9 mm
Nylon	11.3–22.6 mm	7.6–12.6 mm	5.1–8.5 mm
PLA	2.8–5.6 mm	1.9–3.1 mm	1.3–2.1 mm
PC	3.1–6.1 mm	2.3–3.8 mm	1.6–2.6 mm
PA6-GF25	1.5–2.9 mm	1.0–1.6 mm	0.7–1.1 mm
PA6-CF20	0.9–1.8 mm	0.6–1.0 mm	0.4–0.7 mm

Figure 8 summarizes the key characteristics taken into consideration in the analysis: material cost, weight, printing time, UTS, and rigidity. The figure represents a collection of customized polymer and composite wrist splints in AM characterized by the minimum thickness that allows the part to resist the simulated accidental impact. Precisely, the considered splint configurations were ABS and nylon with a 4 mm surface thickness, PLA and PC with a 3 mm surface thickness, and PA6-GF25 and PA6-CF20 with a 2 mm thickness. The final selection of the six different combinations of materials and thicknesses was based on the safety factor, a numerical value calculated by dividing the UTS of the material by the maximum expected stress experienced by the medical device (respectively to 64 MPa for a splint configuration of 2 mm, 28 MPa for a splint configuration of 3 mm, and 18 MPa for a splint configuration of 4 mm). The considered safety factor was 1.25, and according to some literature studies [49,50], it was identified as the appropriate minimum value for rehabilitation devices. Regarding the nylon splint, this arrangement was included for comparative purposes only in light of the inadequate results obtained from the displacement distribution maps.

3.2. Discussion

The analyses conducted on the printing times of the wrist immobilization splints showed that with the considered 3D printing technology (Ultimaker S5 FDM), the material deposition time varied significantly depending on the selected material type and layer thickness. In particular, the material deposition time ranged from a minimum of 2.2 h and a maximum of 6.4 h.

The analysis conducted with the slicing software demonstrated that the estimated times were the result of the sum of multiple components, and the overall time value was attributable to a few leading time components, such as the outer and inner wall deposition and retractions (movement of the head nozzle with the function of avoiding the stringing effect). The time component related to the deposition of the support material did not fit into the aforementioned leading time components since its value was modest as a result of the optimized printing parameters (support overhang angle = 80°) and optimized printing orientation (vertical orientation in the top right quadrant of the printing plane). In fact, for each splint configuration, the recorded support value was always below 8% of the whole printing time.

The composite materials, PA6-GF25 and PA6-CF20, presented by far the highest printing values due to a technical constraint: a narrower FDM nozzle diameter resulted in a reduction in the deposited layer height from 0.6 mm to 0.45 mm. Thus, composite materials demanded a printing time of at least 4.5 h just to realize the thinnest thickness (2 mm). In contrast, for the same level of thickness, the polymeric materials required a shorter printing time, ranging from 2.2 h to 2.8 h. Additionally, the composite printing time was lengthened by the post-printing annealing: it is recommended to anneal (oven at 90 °C for 2 h) the composite prototypes to improve their mechanical and thermal properties. Polymeric prototypes do not require any annealing processes.

With respect to the cost analysis, the value of the total material cost was given by the sum of the manufacturing material and support material cost components. The aggregate material cost ranged from 6 EUR for 2 mm thickness wrist splints manufactured with ABS or PLA to over 30 EUR for 4 mm thickness wrist splints made of composite material.

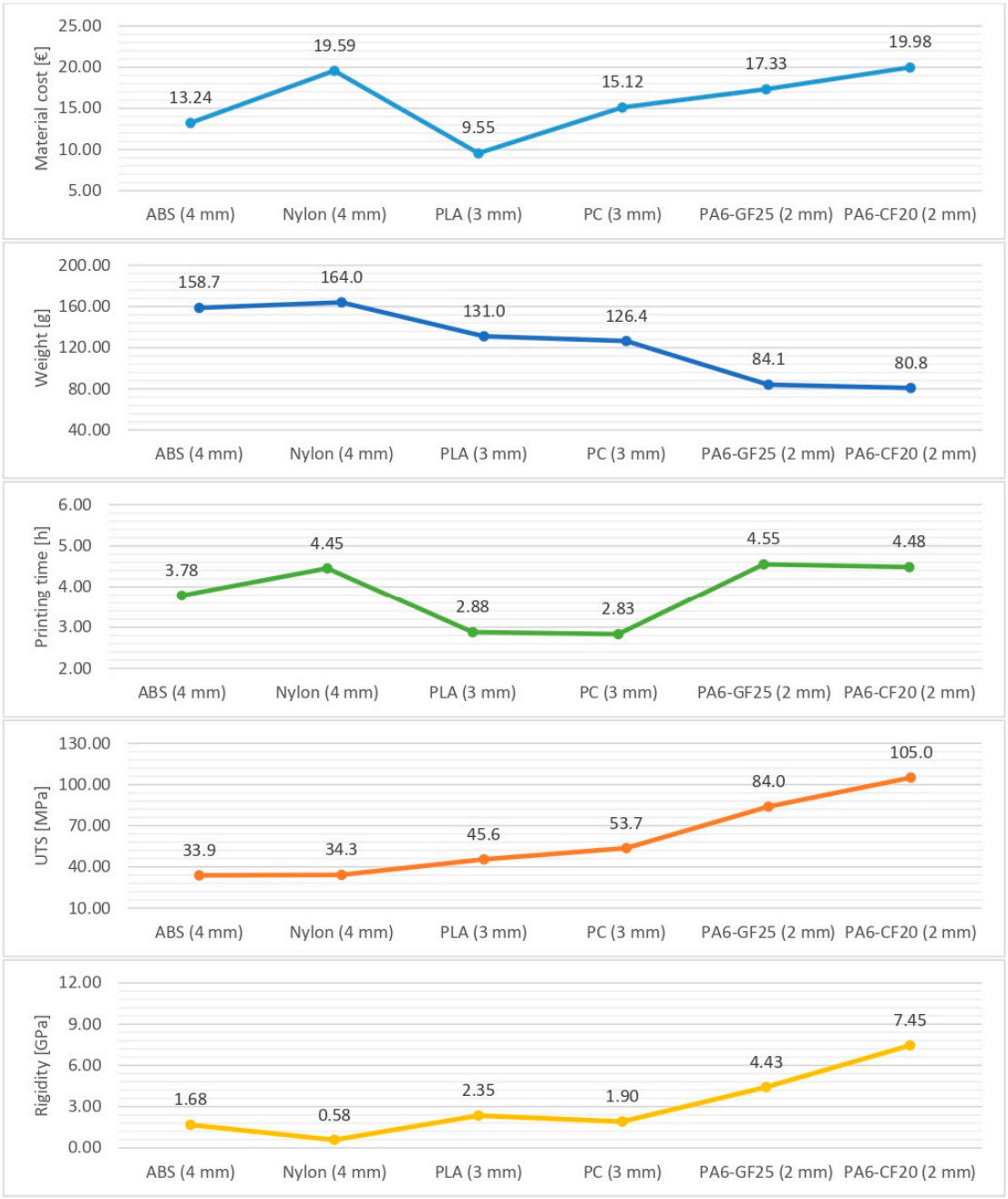

Figure 8. Comparison of the main characteristics of the wrist immobilization splint made in polymeric and composite materials.

Comparably to the above-mentioned discussion on the deposition time of the support material, the contribution of the support material component to the total material cost was almost negligible as the amount of support material extruded was minimized. The amount of deposited support material might be subjected to variations due to its close dependence on the model geometry resulting from the scanning and modeling activities. In the present instance, deposition of the support material occurred only at the closures and the opening area dedicated to the thumb finger. The following designs of fastening systems should focus on the realization of systems involving elements that do not protrude from the primary splint structure (e.g., an interlocking closure on the interaction surfaces of the two splint shells). Further adjustments to the opening dedicated to the thumb finger are desirable: the shape of the thumb opening must limit the creation of downward-facing surfaces. These improvements would assure the complete removal of the supporting

material, thus eliminating all the issues related to the use of the support material, primarily the prolonged printing time and the rougher surface finish of the areas in contact with the support. Although the support material was used, the main structure of the wrist immobilization splint was still able to self-support during the 3D printing activity.

As a result of the cost and time assessments on the innovative methodology, an advantage in terms of material cost was evident compared to traditional splinting, both prefabricated splints and tailor-made splints. Concerning production time, the 3D printing times were substantial, thus making the innovative methodology unfavorable compared to conventional solutions at first glance. To some extent, this drawback might be mitigated through the use of more performant AM technologies that are able to reduce material deposition time. Notwithstanding, when comparing the production times of the traditional procedure with the AM methodology, additional remarks that deviate from the mere amount of time should be made. In particular, it should be noted that the medical application under investigation addresses non-emergency clinical conditions (such as carpal tunnel syndrome, tendinitis, and arthritis). Therefore, from a clinical point of view, there are no real drawbacks associated with the prolonged production time. With no time constraint, the medical solution might be delivered to the patient at a later time (e.g., after an election visit or after a surgical operation) following the limb scanning and splint design. In support of this thesis, it must be noted that the physician's contribution lies in the scanning and modeling activities. In fact, the active presence of the physician during the 3D printing phase is not mandatory (except for the start-up and the shutdown of the AM machine), as the process is fully automated. Along with the discussion of the applicability and sustainability of the AM splinting process within the clinical practice viewed in terms of production time and material costs, technical aspects aimed at defining the feasibility and functionality of the derived medical devices were considered. Simulations determined the opening area dedicated to the thumb finger as the area of potential fracture. Wrist splint configurations unable to withstand accidental mechanical impact (500 N) were excluded as inadequate at providing a sufficient immobilization function of the wrist joint. The prototypes fabricated with composite materials (PA6-GF25 and PA6-CF20) were the only splint configurations able to resist the simulated mechanical impact at every surface thickness. As for prototypes fabricated with polymeric material (ABS, nylon, PLA, PC), the splint configurations with the smallest surface thickness (2 mm) were not achievable because the maximum recorded stress value exceeded the material UTS. By increasing the thickness to 3 mm, all polymeric prototypes were able to withstand the impact. However, it should be noted that in some cases, like the ABS and nylon prototypes, the maximum stress values were not so different from their UTS such that it is preferable to discard these solutions in favor of wrist splint configurations characterized by a greater thickness. From the stress distribution assessment, the selected splint configurations were ABS and nylon with a 4 mm surface thickness, PLA and PC with a 3 mm surface thickness, and PA6-GF25 and PA6-CF20 with a 2 mm surface thickness.

In addition to the simulations that determined whether the wrist immobilization splint undergoes a rupture, considerable importance was paid to the displacement parameter. The ability of the medical device to provide an adequate immobilization function must assume a limited value of element displacements from their initial location during the execution of the accidental mechanical impact. Technical evaluations reported that the greatest displacement was recorded in correspondence to the extremity of the palm with considerably less impact on the wrist area. As expected, a lower surface thickness exhibited greater displacements. Under the same value of surface thickness, materials characterized by greater flexibility exhibited greater displacements. Specifically, excessive displacement values were registered in customized wrist splints made of nylon (including the configuration presenting a surface thickness of 4 mm), thus undermining their effective immobilization functionality.

Along with the stress and displacement distribution maps, other technical aspects (generally sought by the physician during the traditional fabrication of a customized splint) were involved in the discussion. Observations were made on the conformability and design appearance (e.g., ventilation and thickness) aspects.

Conformability, or the ability of the splint to intimately fit the patient's arm, no longer depends on the choice of LTT material and the physician's expertise. Conformability is intrinsic to the process as the customized device is nothing more than a replica of the morphology of the patient's arm.

Another aspect concerned the perforations, which are intended to favor air exchange while simultaneously reducing the weight of the medical device. Although several LTT materials with various perforation patterns are commercially available, the use of these materials requires extra precaution (e.g., LTT stretching should be limited to not distort hole patterns nor impact the forecasted pressure and strength distribution). The implementation of ventilation holes was facilitated and standardized in the design of a customized splint via AM. Recalling the objective of this study and taking into consideration that the stresses to which the splint was subjected were concentrated in a small portion of the hole, the adoptable configuration was the one with rhomboid-shaped ventilation holes. Other geometries of ventilation holes, such as ellipsoidal or rectangular holes with rounded corners, completely reduced the effect of stress concentrations. However, it should be envisaged that these configurations require the use of additional support material near the holes to avoid the collapse of the structure during printing, thus increasing the 3D printing time. The pattern of rhomboid-shaped ventilation holes was distributed over the front and back surface of the wrist immobilization splint away from the joining zone of the two halves. Future research should take into consideration the possibility of optimizing the hole distribution according to topology, meaning that the configuration should maximize lightness as a function of strength.

A last consideration regarded surface thickness: commonly, the thickness of a film of LTT material is about 3 mm even if thicknesses of 2 and 4 mm are available as well. The customized AM wrist splints achieved thicknesses comparable to those realized with LTT materials with the advantage that the choice of thickness depended only on the desired level of strength and not on the expertise of the medical operator. Conversely, regarding customized orthoses with LTT materials, it is recommended that physicians with less experience use greater thicknesses, as these are more easily moldable.

As anticipated in Section 3.1 (Figure 8), all the quantitative results derived from the analyses were gathered together in a comprehensive diagram that may assist medical operators in the process of selecting the most appropriate configuration of a wrist splint according to some key characteristics: material cost, weight, printing time, UTS, and rigidity. Although, from the comparative analysis of each variable, wide differences in the splint configuration chosen were visible, in reality, there was no splint configuration that prevailed in absolute terms.

To conclude, the first 3D-printed prototype for wrist splint immobilization is presented in Figure 9: the shells were not subjected to surface treatments, and the closure system was integrated with elastomer rings.

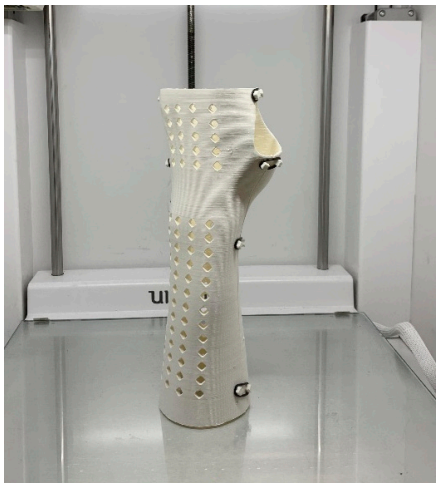

Figure 9. Prototype of wrist immobilization splint made of PLA with a 3 mm surface thickness.

4. Conclusions

The present study developed an innovative manufacturing technique for designing and fabricating highly customized wrist immobilization splints. The process integrated the concepts of RE and AM to overcome the issues associated with conventional prefabricated and tailor-made splints and their manufacturing techniques. In particular, the newly developed methodology addresses the variability induced by different levels of medical expertise by structuring and standardizing the splinting process while providing medical devices characterized by a steady high standard of quality and a high degree of customization.

The commercial availability of different thermoplastic materials allowed the physician to further tailor the splint, keeping in mind that the selection of the most suitable material involved a comparison of the therapeutic targets (specific to a pathological wrist condition) to a series of additional aspects, ranging from the cost and time dimensions to the technical dimension. In this regard, the present study proposed a model for conducting a comparison of the different wrist immobilization configurations that may assist medical operators in choosing the most suitable solution. From the comparative analysis, no splint configuration prevailed over the others. Additionally, cost analyses demonstrated the competitivity of the proposed methodology and medical solutions compared to the traditional procedure, while the advantages related to production time were arguable.

Future works will focus on the aspect of product optimization. Specifically, new designs of fastening systems will be revised. Additionally, refining the wrist immobilization splint will be investigated through the execution of topological optimization; starting from an initial design, the simulation will be aimed at minimizing the overall weight or volume of the wrist splint while ensuring mechanical strength.

Author Contributions: F.S.: execution of the tests and software simulations, data analysis and interpretation of the results, drafting of the manuscript; G.D.: conception and design of the work, final approval of the manuscript; C.G.: data analysis and interpretation of the results, critical revision of the manuscript. All authors have read and agreed to the published version of the manuscript.

Funding: This research received no external funding.

Institutional Review Board Statement: Not applicable.

Informed Consent Statement: Not applicable.

Data Availability Statement: The data that support the findings of this study are available on request from the corresponding author, upon reasonable request.

Conflicts of Interest: The authors declare no conflict of interest.

References

1. Anderson, K.; Anderson, L.E.; Glanze, W.D. *Mosby's Medical, Nursing, & Allied Health Dictionary*; Mosby: Maryland Heights, MO, USA, 1998; ISBN 0815148003.
2. American Society of Hand Therapies. *Splint Classification System*; The American Society of Hand Therapists: Garner, NC, USA, 1992.
3. Bailey, J.; Cannon, N.; Colditz, J.; Fess, E.; Gettle, K.; DeMott, L. *Splint Classification System*; The American Society of Hand Therapists: Garner, NC, USA, 1992.
4. Coppard, B.M.; Lohman, H. *Introduction to Splinting: A Clinical Reasoning and Problem-Solving Approach*; Mosby: Maryland Heights, MO, USA, 2008; ISBN 0323033849.
5. Boyd, A.S.; Benjamin, H.J.; Asplund, C. Principles of Casting and Splinting. *Am. Fam. Physician* **2009**, *79*, 16–22.
6. Paterson, A.M.; Bibb, R.; Campbell, R.I.; Bingham, G. Comparing Additive Manufacturing Technologies for Customised Wrist Splints. *Rapid Prototyp. J.* **2015**, *21*, 230–243. [CrossRef]
7. Althoff, A.D.; Reeves, R.A. *Splinting*; StatPearls Publishing: St. Petersburg, FL, USA, 2022.
8. Wang, Y.; Tan, Q.; Pu, F.; Boone, D.; Zhang, M. A Review of the Application of Additive Manufacturing in Prosthetic and Orthotic Clinics from a Biomechanical Perspective. *Engineering* **2020**, *6*, 1258–1266. [CrossRef]
9. Halanski, M.; Noonan, K.J. Cast and Splint Immobilization: Complications. *J. Am. Acad. Orthop. Surg.* **2008**, *16*, 30–40. [CrossRef] [PubMed]
10. Paoli, A.; Neri, P.; Razionale, A.V.; Tamburrino, F.; Barone, S. Sensor Architectures and Technologies for Upper Limb 3d Surface Reconstruction: A Review. *Sensors* **2020**, *20*, 6584. [CrossRef] [PubMed]

11. TUDelft 3D Handscanner. Available online: https://www.tudelft.nl/en/ide/research/research-labs/applied-labs/3d-handscanner (accessed on 9 August 2023).
12. Carfagni, M.; Furferi, R.; Governi, L.; Servi, M.; Uccheddu, F.; Volpe, Y.; Mcgreevy, K. Fast and Low Cost Acquisition and Reconstruction System for Human Hand-Wrist-Arm Anatomy. *Procedia Manuf.* **2017**, *11*, 1600–1608. [CrossRef]
13. Buonamici, F.; Furferi, R.; Governi, L.; Lazzeri, S.; McGreevy, K.S.; Servi, M.; Talanti, E.; Uccheddu, F.; Volpe, Y. A Practical Methodology for Computer-Aided Design of Custom 3D Printable Casts for Wrist Fractures. *Vis. Comput.* **2020**, *36*, 375–390. [CrossRef]
14. Li, J.; Tanaka, H. Feasibility Study Applying a Parametric Model as the Design Generator for 3D–Printed Orthosis for Fracture Immobilization. *3D Print. Med.* **2018**, *4*, 1. [CrossRef] [PubMed]
15. Oh, I.; Ko, K.H. Automated Recognition of 3D Pipelines from Point Clouds. *Vis. Comput.* **2021**, *37*, 1385–1400. [CrossRef]
16. Divi, S.C.; Verhoosel, C.V.; Auricchio, F.; Reali, A.; Harald Van Brummelen, E. Topology-Preserving Scan-Based Immersed Isogeometric Analysis. *Comput. Methods Appl. Mech. Eng.* **2022**, *392*, 114648. [CrossRef]
17. Passieux, J.-C.; Bouclier, R.; Weeger, O. Image-Based Isogeometric Twins of Lattices with Virtual Image Correlation for Varying Cross-Section Beams. *Int. J. Numer. Methods Eng.* **2023**, *124*, 2237–2260. [CrossRef]
18. Sala, F.; Carminati, M.; D'Urso, G.; Giardini, C. A Feasibility Analysis of a 3D Customized Upper Limb Orthosis. *Procedia CIRP* **2022**, *110*, 207–212. [CrossRef]
19. Baronio, G.; Harran, S.; Signoroni, A. A Critical Analysis of a Hand Orthosis Reverse Engineering and 3D Printing Process. *Appl. Bionics Biomech.* **2016**, *2016*, 8347478. [CrossRef] [PubMed]
20. Lin, H.; Shi, L.; Wang, D. A Rapid and Intelligent Designing Technique for Patient-Specific and 3D-Printed Orthopedic Cast. *3D Print. Med.* **2016**, *2*, 4. [CrossRef] [PubMed]
21. Chen, Y.-J.; Lin, H.; Zhang, X.; Huang, W.; Shi, L.; Wang, D. Application of 3D–Printed and Patient-Specific Cast for the Treatment of Distal Radius Fractures: Initial Experience. *3D Print. Med.* **2017**, *3*, 11. [CrossRef]
22. Mehrpouya, M.; Dehghanghadikolaei, A.; Fotovvati, B.; Vosooghnia, A.; Emamian, S.S.; Gisario, A. The Potential of Additive Manufacturing in the Smart Factory Industrial 4.0: A Review. *Appl. Sci.* **2019**, *9*, 3865. [CrossRef]
23. Ramos, N.; Mittermeier, C.; Kiendl, J. Experimental and Numerical Investigations on Heat Transfer in Fused Filament Fabrication 3D-Printed Specimens. *Int. J. Adv. Manuf. Technol.* **2022**, *118*, 1367–1381. [CrossRef]
24. Moradi, M.; Aminzadeh, A.; Rahmatabadi, D.; Hakimi, A. Experimental Investigation on Mechanical Characterization of 3D Printed PLA Produced by Fused Deposition Modeling (FDM). *Mater. Res. Express* **2021**, *8*, 035304. [CrossRef]
25. Zharylkassyn, B.; Perveen, A.; Talamona, D. Effect of Process Parameters and Materials on the Dimensional Accuracy of FDM Parts. *Mater. Today Proc.* **2021**, *44*, 1307–1311. [CrossRef]
26. Visscher, D.O.; te Slaa, S.; Jaspers, M.E.; van de Hulsbeek, M.; Borst, J.; Wolff, J.; Forouzanfar, T.; van Zuijlen, P.P. 3D Printing of Patient-Specific Neck Splints for the Treatment of Post-Burn Neck Contractures. *Burn. Trauma* **2018**, *6*, 15. [CrossRef]
27. Sabyrov, N.; Sotsial, Z.; Abilgaziyev, A.; Adair, D.; Ali, M.H. Design of a Flexible Neck Orthosis on Fused Deposition Modeling Printer for Rehabilitation on Regular Usage. *Procedia Comput. Sci.* **2021**, *179*, 63–71. [CrossRef]
28. Dombroski, C.E.; Balsdon, M.E.R.; Froats, A. The Use of a Low cost 3D Scanning and Printing Tool in the Manufacture of Custom-Made Foot Orthoses: A Preliminary Study. *BMC Res. Notes* **2014**, *7*, 443. [CrossRef] [PubMed]
29. Walbran, M.; Turner, K.; Mcdaid, A.J. Customized 3D Printed Ankle-Foot Orthosis with Adaptable Carbon Fibre Composite Spring Joint under a Creative Commons Attribution (CC-BY) 4.0 License Customized 3D Printed Ankle-Foot Orthosis with Adaptable Carbon Fibre Composite Spring Joint. *Cogent Eng.* **2016**, *3*, 1227022. [CrossRef]
30. Jin, H.; Xu, R.; Wang, S.; Wang, J. Use of 3D-Printed Heel Support Insoles Based on Arch Lift Improves Foot Pressure Distribution in Healthy People. *Med. Sci. Monit.* **2019**, *25*, 7175. [CrossRef]
31. Xu, R.; Wang, Z.; Ma, T.; Ren, Z.; Jin, H. Effect of 3D Printing Individualized Ankle-Foot Orthosis on Plantar Biomechanics and Pain in Patients with Plantar Fasciitis: A Randomized Controlled Trial. *Med. Sci. Monit.* **2019**, *25*, 1392–1400. [CrossRef]
32. Kim, S.J.; Kim, S.J.; Cha, Y.H.; Lee, K.H.; Kwon, J.Y. Effect of Personalized Wrist Orthosis for Wrist Pain with Three-Dimensional Scanning and Printing Technique: A Preliminary, Randomized, Controlled, Open-Label Study. *Prosthet. Orthot. Int.* **2018**, *42*, 636–643. [CrossRef]
33. Portnova, A.A.; Mukherjee, G.; Peters, K.M.; Yamane, A.; Steele, K.M. Design of a 3D-Printed, Open-Source Wrist-Driven Orthosis for Individuals with Spinal Cord Injury. *PLoS ONE* **2018**, *13*, e0193106. [CrossRef]
34. Lee, K.H.; Kim, D.K.; Cha, Y.H.; Kwon, J.Y.; Kim, D.H.; Kim, S.J. Personalized Assistive Device Manufactured by 3D Modelling and Printing Techniques. *Disabil. Rehabil. Assist. Technol.* **2019**, *14*, 526–531. [CrossRef]
35. Hexagon AB. Hexagon—Empowering an Autonomous, Sustainable Future. Available online: https://hexagon.com (accessed on 9 August 2023).
36. *ISO 10993-1:2018*; Biological Evaluation of Medical Devices. ISO (International Organization for Standardization): Geneva, Switzerland, 2018.
37. Cber, C. *Use of International Standard ISO 10993-1, "Biological Evaluation of Medical Devices-Part 1: Evaluation and Testing within a Risk Management Process" Guidance for Industry and Food and Drug Administration Staff Preface Public Comment*; Center for Devices and Radiological Health: Silver Spring, MD, USA, 2020.
38. Ultimaker Ultimaker ABS—Technical Data Sheet. Available online: https://ultimaker.my.salesforce.com/sfc/p/#j0000000HOnW/a/5b000004UX1e/ymaTcu23yezPH0a2.9qJEJYtA_pvXVnTcQMeWNRiIaY (accessed on 9 August 2023).

39. Ultimaker Ultimaker Nylon—Technical Data Sheet. Available online: https://ultimaker.my.salesforce.com/sfc/p/#j0000000HOnW/a/5b000004UiEo/LIYV6VDfKlwDuaqc.9FhLVGIN0sN96YivUwV0fu7ylA (accessed on 9 August 2023).
40. Ultimaker Ultimaker PLA—Technical Data Sheet. Available online: https://ultimaker.my.salesforce.com/sfc/p/#j0000000HOnW/a/5b000004Uiac/95CBv380plulni.oGx.QVyYZTOIJAc6d_BypJjAmeok (accessed on 9 August 2023).
41. Ultimaker Ultimaker PC—Technical Data Sheet. Available online: https://ultimaker.my.salesforce.com/sfc/p/#j0000000HOnW/a/5b000004TlDg/NmLGE1iImMnHn_5T0YLumlngSpw3CsXc3.ge1aCf_mE (accessed on 9 August 2023).
42. Polymaker PolyMide PA6-GF—Technical Data Sheet. Available online: https://c-3d.niceshops.com/upload/file/PolyMide_PA6_GF_TDS_V5.1.pdf (accessed on 9 August 2023).
43. Polymaker PolyMide PA6-CF—Technical Data Sheet. Available online: https://c-3d.niceshops.com/upload/file/PolyMide_PA6_CF_TDS_V5.1.pdf (accessed on 9 August 2023).
44. Ultimaker Ultimaker Breakaway—Technical Data Sheet. Available online: https://ultimaker.my.salesforce.com/sfc/p/#j0000000HOnW/a/5b000004Udwf/FxKwB7aukJUO6tPWfTUYr089QQMY3u1bPhreKFrXDs4 (accessed on 9 August 2023).
45. Ultimaker Recommended Printing Settings and Configurations for Ultimaker ABS. Available online: https://support.makerbot.com/s/article/1667337602935 (accessed on 9 August 2023).
46. Ultimaker Recommended Printing Settings and Configurations for Ultimaker Nylon. Available online: https://support.makerbot.com/s/article/1667337602768 (accessed on 9 August 2023).
47. Ultimaker Reccomended Printing Settings and Configurations for Ultimaker PLA. Available online: https://support.makerbot.com/s/article/1667337611872 (accessed on 9 August 2023).
48. Ultimaker Recommended Printing Settings and Configurations for Ultimaker PC. Available online: https://support.makerbot.com/s/article/1667337602519 (accessed on 9 August 2023).
49. Brett, A.M. Fatigue Failures. In *ASM International Handbook Failure Analysis and Prevention.*; Becker, W.T., Shipley, R.J., Eds.; ASM International: Russell Township, OH, USA, 2002; Volume 11.
50. Reis, P.; Volpini, M.; Pimenta Maia, J.; Batista Guimarães, I.; Evelise, C.; Monteiro, M.; Carlos Campos Rubio, J. Resting Hand Splint Model from Topology Optimization to Be Produced by Additive Manufacturing. *Rapid Prototyp. J.* **2022**, *28*, 216–225. [CrossRef]